
Random Teachers are Good Teachers

Felix Santhein¹ Gregor Bachmann¹ Sotiris Anagnostidis¹ Thomas Hofmann¹

Abstract

In this work, we investigate the implicit regularization induced by teacher-student learning dynamics. To isolate its effect, we describe a simple experiment where instead of trained teachers, we consider teachers at random initialization. Surprisingly, when distilling a student into such a random teacher, we observe that the resulting model and its representations already possess very interesting characteristics; (1) we observe a strong improvement of the distilled student over its teacher in terms of probing accuracy. (2) The learnt representations are highly transferable between different tasks but deteriorate strongly if trained on random inputs. (3) The student checkpoint suffices to discover so-called lottery tickets, i.e. it contains identifiable, sparse networks that are as performant as the full network. These observations have interesting consequences for several important areas in machine learning: (1) Self-distillation can work solely based on the implicit regularization present in the gradient dynamics without relying on any *dark knowledge*, (2) self-supervised learning can learn features even in the absence of data augmentation and (3) SGD already becomes stable when initialized from the student checkpoint with respect to batch orderings. Finally, we shed light on an intriguing local property of the loss landscape: the process of feature learning is strongly amplified if the student is initialized closely to the teacher. This raises interesting questions about the nature of the landscape that have remained unexplored so far.

1. Introduction

The teacher-student setting is a key ingredient in several areas of machine learning. Knowledge distillation is a common strategy to achieve strong model compression by training a smaller student on the outputs of a larger teacher model, leading to better performance compared to training

the small model on the original data only (Bucila et al., 2006; Ba & Caruana, 2013; Hinton et al., 2015; Polino et al., 2018; Yim et al., 2017; Chen et al., 2017). In the special case of self-distillation, where the two architectures match, it is often observed in practice that the student manages to outperform its teacher (Zhang et al., 2019; Furlanello et al., 2018; Yang et al., 2018). The pre-dominant hypothesis in the literature attests this surprising gain in performance to the so-called *dark knowledge* of the teacher, i.e. its logits encode additional information about the data distribution (Hinton et al., 2015; Wang et al., 2021; Xu et al., 2018).

Another area relying on a teacher student setup is non-contrastive self-supervised learning where the goal is to learn informative representations in the absence of targets (Caron et al., 2021a; Grill et al., 2020; Chen & He, 2021; Zbontar et al., 2021; Assran et al., 2022). Here, the two models typically receive two different augmentations of a sample and the student is forced to mimic the behaviour of the teacher. Such a learning strategy encourages representations that remain invariant to the employed augmentation pipeline, which in turn leads to better downstream performance.

Despite its importance as a building block, the teacher-student setting itself remains very difficult to analyze as its contribution is often overshadowed by stronger components in the pipeline such as *dark knowledge* in the trained teacher or the inductive bias of data augmentation. In this work we take a step towards simplifying and isolating the key components in the setup by devising a very simple experiment; instead of working with a trained teacher, we consider teachers at random initialization, stripping them from any data-dependence and thus removing any *dark knowledge*. We also remove augmentations, making the setting completely symmetric between student and teacher and further reducing inductive bias. Counter-intuitively, we observe that even in this setting, the student still manages to learn from its teacher and even exceed it significantly in terms of representational quality, measured through linearly probing the features (see Fig. 1). This result shows the following: (1) Even in the absence of *dark knowledge*, relevant feature learning can happen for the student in the setting of self-distillation. (2) Data augmentation is the main but not only ingredient in non-contrastive self-supervised learning that leads to representation learning.

Surprisingly, we find that initializing the student close to the

¹Department of Computer Science, ETH Zürich, Switzerland. Correspondence to: Felix Santhein <safelix@ethz.ch>.

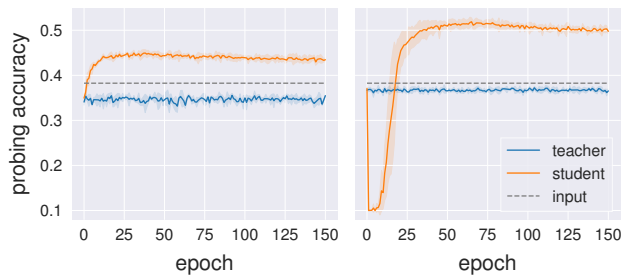


Figure 1. Linear probing accuracies of representations generated by teachers, students, and the flattened input images on *CIFAR10* as a function of training time. **Left:** *ResNet18*. **Right:** *VGG11* without batch normalization.

teacher further amplifies the implicit regularization present in the dynamics. This is in-line with common practices in non-contrastive learning, where teacher and student are usually initialized closely together and only separated through small asymmetries in architecture and training protocol (Grill et al., 2020; Caron et al., 2021a; Tarvainen & Valpola, 2017). We study this locality effect of the landscape and connect it with the ‘asymmetric valleys’ phenomenon observed in He et al. (2019a).

Inspired by the improvement in terms of probing accuracy, we study the converged student checkpoint as an initialization for sparse network discovery. Similarly to Frankle et al. (2020b), we find that so-called lottery tickets are already contained in the student and no additional gradient steps are necessary to unravel them, in contrast to Frankle & Carbin (2019); Frankle et al. (2020a) where training on the concrete learning tasks for a few epochs is essential.

2. Related Work

There are several works in the literature aiming at analyzing self-distillation and the impact on the student. Phuong & Lampert (2019) prove a generalization bound that establishes fast decay of the risk in case of linear models. Mobahi et al. (2020) demonstrate an increasing regularization effect through repeated distillation for kernel regression. Ji & Zhu (2020) consider a similar approach and rely on the fact that very wide networks behave very similarly to the neural tangent kernel (Jacot et al., 2018) and leverage this connection to establish risk bounds. Allen-Zhu & Li (2020) on the other hand study more realistic width networks and show that if the data satisfies a certain multi-view property, ensembling and distilling is provably beneficial. Yuan et al. (2020) study a similar setup as our work by considering teachers that are not perfectly pre-trained but of weaker (but still far from random) nature. They show that the *dark knowledge* is more a regularization effect and that a similar boost in performance can be achieved by label smoothing. We would like to point out however that we study completely random

teachers and our loss function does not provide the hard labels for supervisory signal, making our task completely independent of the targets. Another related work studies *benign memorization* (Anagnostidis et al., 2022) where it is shown that strong representation learning can happen even if the targets are replaced by random labels. In contrast to our work, the authors rely on heavy data augmentation and hence no implicit regularization is contained in the dynamics due to the random labels.

Self-supervised learning can be broadly split into two categories, contrastive and non-contrastive methods. Contrastive methods rely on the notion of negative examples, where features are actively being encouraged to be dissimilar if they stem from different examples (Chen et al., 2020; Schroff et al., 2015; van den Oord et al., 2018). Non-contrastive methods follow our setting more closely as only the notion of positive examples is employed (Caron et al., 2021a; Grill et al., 2020; Chen & He, 2021). While these methods enjoy great empirical successes, a theoretical understanding is still largely missing. Tian et al. (2021) investigate the collapse phenomenon in non-contrastive learning and show in a simplified setting how the stop gradient operation can prevent it. Wang et al. (2022) extend this work and prove in the linear setting how a data-dependent projection matrix is learnt. Zhang et al. (2022) explore a similar approach and prove that *SimSiam* (Chen & He, 2021) avoids collapse through the notion of extra-gradients. Despite this progress on the optimization side, a good understanding of feature learning has largely remained elusive.

The high-dimensional loss landscapes of neural networks remain very mysterious and their properties play a crucial role in our work. While some structures of it such as (lack of) linear-mode connectivity and low test loss curves between minima are well-understood (Garipov et al., 2018; Frankle et al., 2020a; Draxler et al., 2018; Nagarajan & Kolter, 2019), the field still lacks a convincing explanation as to how simple first-order gradient-based methods such as SGD manage to navigate the landscape so efficiently. In our experiments, we encounter a novel, *local* property of the loss landscape, where a precise initialization turns out to be essential for successful downstream performance.

3. Setting

Notation. Let us setup some notation first. We consider a family of parametrized functions $\mathcal{F} = \{f_{\theta} : \mathbb{R}^d \rightarrow \mathbb{R}^m \mid \theta \in \Theta\}$ where θ denotes the (vectorized) parameters of a given model and Θ refers to the underlying parameter space. In this work we study the teacher-student setting, i.e. we consider two models f_{θ_T} and f_{θ_S} from the same function space \mathcal{F} . We will refer to f_{θ_T} as the teacher model and to f_{θ_S} as the student model. Notice that here we assume that both teacher and student have the same architecture unless oth-

erwise stated. Moreover, assume that we have access to $n \in \mathbb{N}$ input-output pairs $(\mathbf{x}_1, y_1), \dots, (\mathbf{x}_n, y_n)$ $i.i.d.$ \mathcal{D} distributed according to some probability measure \mathcal{D} , where $\mathbf{x}_i \in \mathbb{R}^d$ and $y_i \in \{0, \dots, K-1\}$ encodes the class membership for one of the $K \in \mathbb{N}$ classes.

Supervised. The standard learning paradigm in machine learning is supervised learning, where a model $f_\theta \in \mathcal{F}$ is chosen based on empirical risk minimization, i.e. given a loss function l , we train a model to minimize

$$L(\theta) := \sum_{i=1}^n l(f_\theta(\mathbf{x}_i), y_i).$$

Minimization of the objective is usually achieved by virtue of standard first-order gradient-based methods such as SGD or ADAM (Kingma & Ba, 2017), where parameters $\theta \sim \text{INIT}$ are randomly initialized and then subsequently updated based on gradient information.

Teacher-Student Loss. A similar but distinct way to perform learning is the teacher-student setting. Here we first fix a teacher model f_{θ_T} where θ_T is usually a parameter configuration arising from training in a supervised fashion on the same task. The task of the student f_{θ_S} is then to mimic the teacher’s behaviour on the training set by minimizing a distance function d between the two predictions,

$$L(\theta_S) := \sum_{i=1}^n d(f_{\theta_S}(\mathbf{x}_i), f_{\theta_T}(\mathbf{x}_i)). \quad (1)$$

We have summarized the setting schematically in Fig. 2. We experiment with several choices for the distance function but largely focus on the KL divergence. We remark that many works on self-distillation (Tarvainen & Valpola, 2017) consider a combination of losses of the form

$$L(\theta_S) := \sum_{i=1}^n d(f_{\theta_S}(\mathbf{x}_i), f_{\theta_T}(\mathbf{x}_i)) + \beta \sum_{i=1}^n l(f_\theta(\mathbf{x}_i), y_i),$$

for $\beta > 0$, thus the objective is also informed by the true labels y . Here we set $\beta = 0$ to precisely test how much performance is solely due to the implicit regularization present in the learning dynamics and the inductive bias of the model.

Somewhat counter-intuitively, it has been observed in many empirical works that the resulting student often outperforms its teacher. It has been hypothesized in many prior works that the teacher logits $f_{\theta_T}(\mathbf{x})$ encode some additional, relevant information for the task that benefit learning (*dark knowledge*), i.e. wrong but similar classes might have a non-zero probability under the teacher model (Hinton et al., 2015; Wang et al., 2021; Xu et al., 2018). In the following, we will explore this hypothesis by systematically destroying the label information in the teacher.

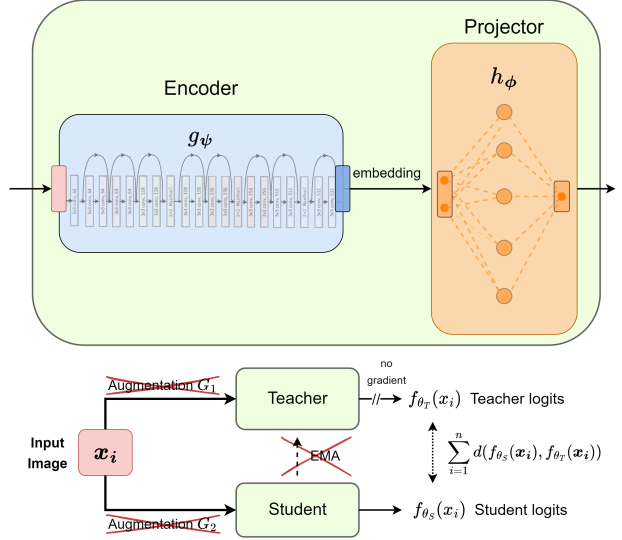


Figure 2. Schematic drawing of the teacher-student setup. The model consists of an encoder and projector. The same image is passed to both student and teacher and the outputs of the projectors are compared. The student weights are then adjusted to mimic the output of the teacher. In this work, we consider a simplified setting without augmentations and without teacher updates such as EMA.

Non-Contrastive. Self-supervised learning is a recently developed methodology enabling the pretraining of vision models on large-scale unlabelled image corpora, akin to the autoregressive loss in natural language processing (Devlin et al., 2019). A subset of these approaches is formed by non-contrastive methods. Consider a set of image augmentations \mathcal{G} where any $G \in \mathcal{G}$ is a composition of standard augmentation techniques such as random crop, random flip, color jittering etc. The goal of non-contrastive learning is to learn a parameter configuration that is invariant to the employed data augmentations while avoiding to simply collapse to a constant function. Most non-contrastive objectives can be summarized to be of the form

$$L(\theta_S) := \sum_{i=1}^n \mathbb{E}_{G_1, G_2} [d(f_{\theta_S}(G_1(\mathbf{x}_i)), f_{\theta_T}(G_2(\mathbf{x}_i)))]$$

where the expectation is taken uniformly over the set of augmentations \mathcal{G} . In Fig. 3 we have summarized this pipeline schematically. While the teacher does not directly receive any gradient information, the parameters θ_T are often updated based on an exponentially weighted moving average,

$$\theta_T \leftarrow (1 - \gamma)\theta_T + \gamma\theta_S$$

which is applied periodically at a fixed frequency. In this work, we will consider a simplified setting without augmentations and where the teacher remains frozen at random initialization, $\gamma = 0$.

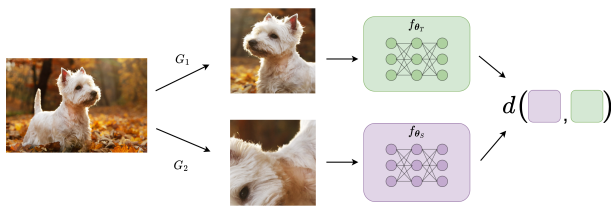


Figure 3. Schematic illustration of non-contrastive learning. Two augmentations are produced and passed to the student and teacher respectively. Then a distance function is minimized to make encourage stronger similarity of the representations.

Probing. Since minimizing the teacher-student loss is a form of unsupervised learning if the teacher itself has not seen any labels, we need a way to measure the quality of the resulting features. Here we rely on the idea of probing representations, a very common technique from self-supervised learning (Chen & He, 2020; Chen et al., 2020; Caron et al., 2021a; Bardes et al., 2022; Grill et al., 2020). As illustrated in Fig. 2, the network is essentially split into an encoder $g_\psi : \mathbb{R}^d \rightarrow \mathbb{R}^r$ and a projector $h_\phi : \mathbb{R}^r \rightarrow \mathbb{R}^m$ where it holds that $f_\theta = h_\phi \circ g_\psi$. The encoder is usually given by the backbone of a large vision model such as *ResNet* (He et al., 2016) or *VGG* (Simonyan & Zisserman, 2014), while the projector is parametrized by a shallow MLP. We then *probe* the representations g_ψ by learning a linear layer on top, where we now leverage the label information y_1, \dots, y_n . Notice that the weights of the encoder remain frozen while learning the linear layer. The idea is that a linear model does not add more feature learning capacity, and the resulting probing accuracy hence provides an adequate measure of quality of the representations. Unless otherwise stated, we perform probing on the *CIFAR10* dataset and aggregate mean and standard deviation over three runs.

4. Random Teacher Distillation

Distillation. Let us denote by $\theta \sim \text{INIT}$ a randomly initialized parameter configuration, according to some standard initialization scheme INIT. Throughout this text, we rely on *Kaiming* initialization (He et al., 2015). In standard self-distillation, the teacher is a parameter configuration $\theta_T^{(l)}$ resulting from training in a supervised fashion for $l \in \mathbb{N}$ epochs on the task $\{(\mathbf{x}_i, y_i)\}_{i=1}^n$. In a next step, the teacher is then distilled into a student, i.e. the student is trained to match the outputs of the pre-trained teacher $f_{\theta_T^{(l)}}$. In this work, we change the nature of the teacher and instead consider a teacher at random initialization $\theta_T \sim \text{INIT}$ (we drop the superscript 0 for convenience). The teacher has thus not seen any data at all and is hence of a similar (bad) quality as the student. This experiment, therefore, serves as the ideal test bed to measure the implicit regularization present in the optimization itself without relying on any *dark knowledge*

about the target distribution. Due to the absence of targets, the setup also closely resembles the learning setting of non-contrastive methods. Through that lens, our experiment can also be interpreted as a non-contrastive pipeline without *augmentations* and exponential moving average.

We minimize the objective (1) with the ADAM optimizer (Kingma & Ba, 2017) using a learning rate $\eta = 0.001$. We analyze two encoder types based on the popular *ResNet18* and *VGG11* architectures and similarly to Caron et al. (2021a), we use a 2-hidden layer MLP with an L_2 bottleneck, as a projector. To assess whether batch-dependent statistics play a role, we remove the batch normalization layers (Ioffe & Szegedy, 2015) from the *VGG11* architecture. For more details on the architecture and hyperparameters, we refer to App. C. We display the linear probing accuracy of both student and teacher as a function of training time in Fig. 1 on the *CIFAR10* dataset (Krizhevsky & Hinton, 2009). We follow the protocol of non-contrastive learning and initialize the student closely to the teacher. We will expand more on this choice of initialization in the next paragraph. Notice that while the teacher remains fixed throughout training, linear probing accuracies can vary due to the stochastic optimization. As a result, we observe that teacher probes exhibit minor fluctuations. The dashed line represents the linear probing accuracy obtained directly from the (flattened) inputs. We clearly see that the student significantly outperforms its teacher throughout the training. Moreover, it also improves over probing on the raw inputs, demonstrating that not simply less signal is lost due to random initialization but rather that meaningful learning is performed. We expand our experimental setup to more datasets, including *CIFAR100* (Krizhevsky & Hinton, 2009), *STL10* (Coates et al., 2011) and *TinyImageNet* (Le & Yang, 2015). We summarize the results in Table 1. We observe that across all tasks, distilling the student into a random teacher proves beneficial in terms of probing accuracy. For further ablations on the architecture, we refer to the App. B. Moreover, we find very similar results for k -NN probing instead of linear in App. D.1.

Local Initialization. It turns out that the initialization of the student and its proximity to the teacher plays a crucial role. To that end, we consider initializations of the form

$$\theta_S(\alpha) = \frac{1}{\delta} \left((1 - \alpha)\theta_T + \alpha\tilde{\theta} \right),$$

where $\tilde{\theta} \sim \text{INIT}$ is a fresh initialization, $\alpha \in [0, 1]$ and $\delta = \sqrt{\alpha^2 + (1 - \alpha)^2}$ ensures that the variance remains constant $\forall \alpha \in [0, 1]$. Values for α close to 0 result in student initializations in close proximity to the teacher configuration. We refer to initializations with small α as *local* initializations and coin α the locality parameter. It is important to point out that in the non-contrastive learning setting, teacher and student are initialized at the exact same parame-

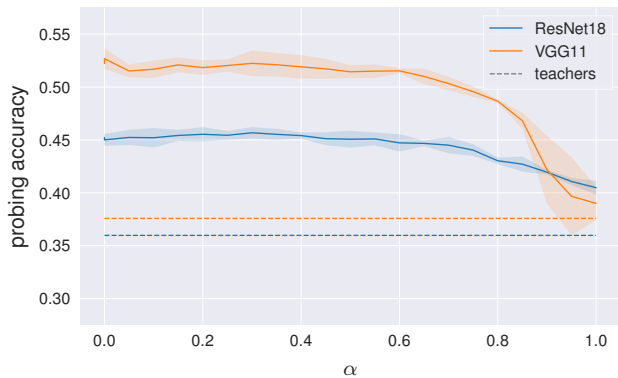


Figure 4. Linear probing accuracies of the encoder $g_{\theta_S^*}(\alpha)$ on *CIFAR10* as a function of the locality parameter α after 150 epochs.

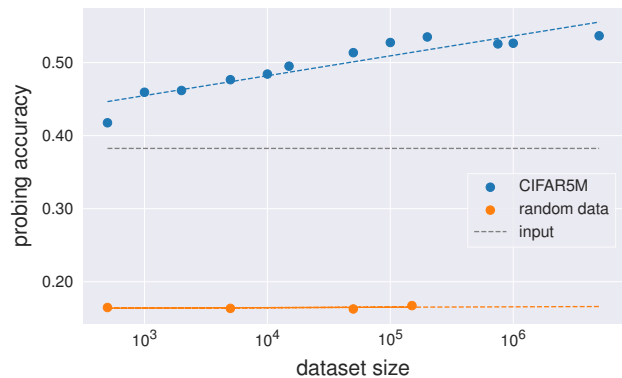


Figure 5. Linear probing accuracy of a *VGG11* trained on *CIFAR5M* and evaluated on *CIFAR10* as a function of sample size.

DATASET	MODEL	TEACHER	STUDENT	INPUT
<i>CIFAR10</i>	<i>ResNet18</i>	35.50	46.02	39.02
	<i>VGG11</i>	36.55	51.98	
<i>CIFAR100</i>	<i>ResNet18</i>	11.58	21.50	14.07
	<i>VGG11</i>	12.05	26.62	
<i>STL10</i>	<i>ResNet18</i>	24.24	40.58	31.51
	<i>VGG11</i>	24.67	46.20	
<i>TinyImageNet</i>	<i>ResNet18</i>	4.85	10.40	3.28
	<i>VGG11</i>	5.25	12.88	

Table 1. Linear probing accuracies (in percentage) of the representations for various datasets for teacher, student and pixel inputs.

ter values (i.e. $\alpha = 0$) and only minor asymmetries in the architectures lead to different overall functions. We now study how the locality parameter α can affect the resulting quality of the representations of the student in our setup. We display the resulting probing accuracy of the teacher as a function of the locality parameter α in Fig. 4. Surprisingly, we find that α has a very pronounced effect on the resulting accuracies, e.g. initializing the student independently of the teacher ($\alpha = 1$) almost entirely destroys the improvement over the teacher. To the best of our knowledge, we are the first to observe such a locality phenomenon in the teacher-student landscape. We investigate this phenomenon in more detail in the next section and for now, if not explicitly stated otherwise, use initializations with small locality parameter $\alpha \sim 10^{-10}$.

Data-dependence. In a next step we aim to better understand the origin of the observed improvement and to what degree the learnt features are data-dependent, i.e. tuned to the particular input distribution $\mathbf{x} \sim p_{\mathbf{x}}$. While the improvement over the raw input probe already suggests non-trivial learning, we want to more precisely characterize the role of

the input data.

As a first experiment, we study how the improvement of the student over the teacher evolves as a function of the sample size n involved in the teacher-student training phase. Notice that for probing, we do not adjust the sample size but always use the standard training set. We use the *CIFAR5M* dataset, where the standard *CIFAR10* dataset has been extended to 5 million data points through the usage of a generative adversarial network (Nakkiran et al., 2021). We train the student for different sample sizes in the interval $[5 \times 10^2, 5 \times 10^6]$ and probe the learnt features on the standard *CIFAR10* training and test set. We display the resulting probing accuracy as a function of sample size in Fig. 5 (blue line). Indeed, we observe a steady increase in performance of the student as the size of the data corpus grows, highlighting that data-specific feature learning is happening. As further confirmation, we next replace the inputs $\mathbf{x}_i \sim p_{\mathbf{x}}$ with pure Gaussian noise, i.e. $\mathbf{x}_i \sim \mathcal{N}(\mathbf{0}, \sigma^2 \mathbf{1})$, effectively removing any relevant structure in the samples. The linear probing on the other hand is again performed on the clean data. This way we can assess whether the teacher-student training is simply moving the initialization in a favorable way (e.g. potentially ‘uncollapsing’ it), which would still prove beneficial for meaningful tasks. We show the probing accuracy as a function of dataset size, for these random inputs, as well in Fig. 5 (orange line). Very clearly, such a random input training does not lead to an improvement of the student, on the contrary, the performance of the student collapses to randomly guessing the targets, across all dataset sizes. This is another indication that data-dependent feature learning is happening, where in this case adapting to the noise inputs of course proves detrimental for the clean probing.

Transferability. As a final measure for the quality of the learnt features, we test how well a set of representations obtained on one task transfers to a related but different task. More precisely, we are given a source task

DATASET	MODEL	TEACHER	STUDENT
CIFAR10	ResNet18	35.50	46.06
	VGG11	36.55	52.45
CIFAR100	ResNet18	11.58	22.60
	VGG11	12.05	27.49
STL10	ResNet18	24.24	41.42
	VGG11	24.67	45.86

Table 2. Linear probing accuracies (in percentage) of the representations for various datasets for teacher and student. The student is trained by distilling a random teacher on the *TinyImageNet* dataset.

$\mathcal{A} = \{(\mathbf{x}_i, y_i)\}_{i=1}^n \stackrel{i.i.d.}{\sim} \mathcal{D}_A$ and a target task $\mathcal{B} = \{(\mathbf{x}_i, y_i)\}_{i=1}^{\tilde{n}} \stackrel{i.i.d.}{\sim} \mathcal{D}_B$. We assume that both tasks are related, i.e. some useful features on \mathcal{A} also prove to be useful on task \mathcal{B} . For our experiments, the two tasks are usually two image-recognition tasks such as *TinyImageNet* and *CIFAR10*. We then first use the source task \mathcal{A} to perform random teacher distillation. We then use the target task \mathcal{B} to train and evaluate the linear probe. Clearly, we should only see an improvement in the probing accuracy over the (random) teacher if the features learnt on the source task encode relevant information for the target task as well. We illustrate the results of such a transfer strategy for various source and task dataset configurations in Table 2.

5. Loss and Probing Landscapes

Visualization. We now revisit the locality property identified in the previous section, where initializations with α closer to zero significantly outperformed other configurations. To gain further insight into the inner-workings of this phenomenon, we visualize the teacher-student loss landscape as well as the resulting probing accuracies as a function of the model parameters. Since the loss function is a very high-dimensional function of the parameters, only "slices" of it can be visualized at once. More precisely, given two directions $\mathbf{v}_1, \mathbf{v}_2$ in parameter space, we form a visualization plane of the form

$$\theta(\lambda_1, \lambda_2) = \lambda_1 \mathbf{v}_1 + \lambda_2 \mathbf{v}_2, \quad (\lambda_1, \lambda_2) \in [0, 1]^2$$

and then collect loss and probing values at a certain resolution. Such visualization strategy is very standard in the literature, see e.g. Li et al. (2018); Garipov et al. (2018); Izmailov et al. (2021). Denote by $\theta_S^*(\alpha)$ the student trained until convergence initialized with locality parameter α . We study two choices for the landscape slices \mathbf{v}_1 and \mathbf{v}_2 ; first we let $\mathbf{v}_1 = \theta_S(1) - \theta_T$ and $\mathbf{v}_2 = \theta_S^*(1) - \theta_T$, i.e. the plane defined by the random teacher θ_T , the student at a fresh, random initialization $\theta_S(1)$ and the resulting trained student $\theta_S^*(1)$. We refer to this choice as the "non-local"

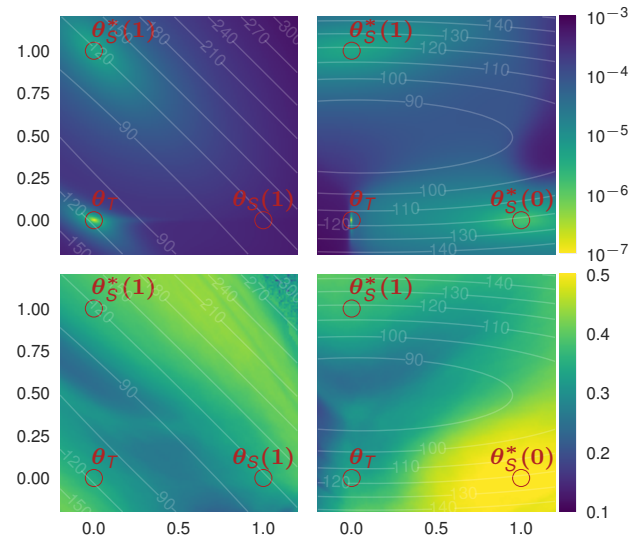


Figure 6. Visualization of the loss and probing landscape. Left column corresponds to the "non-local view" with $\alpha = 1$, whereas the right column contains both the local ($\alpha = 0$) and the non-local solution ($\alpha = 1$). First row displays the loss landscape while the second one shows probing accuracies. Contours lines represent $\|\theta\|_2$, orthogonal projections are in the App. D.2.

view of the landscape since the student is independently initialized from the teacher. The second choice is given by $\mathbf{v}_1 = \theta_S^*(0) - \theta_T$ and $\mathbf{v}_2 = \theta_S^*(1) - \theta_T$, i.e. the plane defined by the random teacher θ_T , the trained student starting from a fresh random initialization $\theta_S^*(1)$ and the trained student $\theta_S^*(0)$ initialized closely to the teacher (α is not exactly zero but around 10^{-10}).

We show the results in Fig. 6, where left and right column represent first and second choice of visualization plane respectively, while first and second row display loss and probing landscapes respectively. For more visualizations, including the loss landscape for the encoder, we refer to App. D.2. Let us focus on the left column first. Clearly, for $\alpha = 1$ the converged student $\theta_S^*(1)$ ends up in a qualitatively different minimum than the teacher (which is the global minimum by definition), i.e. the two points are separated by a significant loss barrier. This is expected as the student is initialized far away from the teacher. Further, we see that the probing landscape is largely unaffected by moving from the initialization $\theta_S(1)$ to the solution $\theta_S^*(1)$, confirming our empirical observation in Fig. 4 that far way initialized students do not improve significantly. The right column reveals more structure. We clearly see that although it was initialized very closely to the teacher, the student $\theta_S^*(0)$ moved considerably. While the energy barrier is smaller as in the case of $\theta_S^*(1)$, it is still very apparent that $\theta_S^*(0)$ settled for a different, local minimum with high probing accuracy. This is surprising as the teacher θ_T itself is the global minimum.

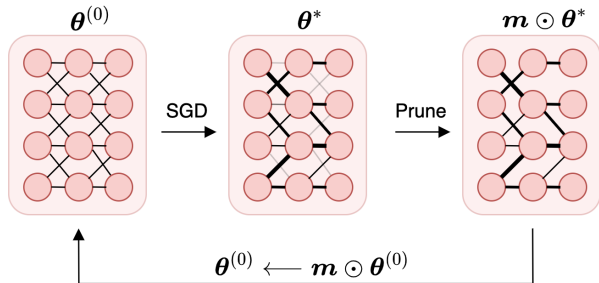


Figure 7. Illustration of the lottery ticket hypothesis and iterative magnitude pruning.

Asymmetric valleys. Another striking structure is the very pronounced asymmetric valley close to the teacher θ_T in the direction of the student $\theta_S^*(0)$, i.e. to the ‘left’, there is a very steep increase in loss while to the ‘right’ it is gradual. On the other hand, we observe that in the probing landscape, walking towards the more flat direction significantly improves probing accuracy. Interestingly, He et al. (2019b) have proven a fact remarkably in-line with our situation. He et al. (2019b) show that being on the flatter side of an asymmetric valley (i.e. $\theta_S^*(0)$) provably leads to better generalization compared to lying in the valley itself (i.e. θ_T). Initializing the student closely to the teacher seems to capitalize on that fact and leads to systematically better generalization. Still, it remains unclear why such an asymmetric valley is only encountered close to the teacher and not for initializations with $\alpha = 1$. We leave a more in-depth analysis of this phenomenon for future work.

6. Discovering Lottery Tickets

Lottery tickets. Another measure to assess the amount of structure present in the student is through sparse network discovery, i.e. the *lottery ticket hypothesis* (Frankle & Carbin, 2019). The lottery ticket hypothesis posits the following: Any large network possesses a sparse subnetwork that can be trained as fast and which achieves or surpasses the test error of the original network. Frankle & Carbin (2019) discover such sparse networks through the following iterative pruning strategy:

1. Fix an initialization $\theta^{(0)} \sim \text{INIT}$ and train a network to convergence in a supervised fashion, leading to θ^* .
2. Prune the parameters based on some criterion, leading to a binary mask m and pruned parameters $m \odot \theta^*$.
3. Prune the initialized network $m \odot \theta^{(0)}$ and re-train.

The above procedure is repeated for a fixed number of times r , and in every iteration, a fraction $k \in [0, 1]$ of

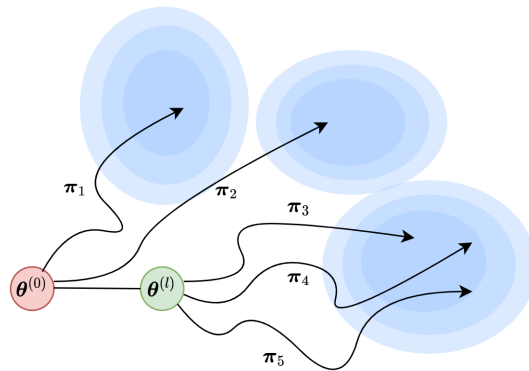


Figure 8. Illustration of stability of SGD and linear mode-connectivity. Blue contour lines indicate a basin of low test loss, π_i denote different batch orderings for SGD.

the weights is pruned, leading to an overall pruning rate of $p_r = \sum_{i=0}^{r-1} (1-k)^i \times k$ percentage of weights. We illustrate the algorithm in Fig. 7. The choice of pruning technique is flexible, in the common variant *iterative magnitude pruning (IMP)* the globally smallest weights are pruned. The above recipe turns out to work very well for MLPs and smaller convolutional networks and indeed very sparse solutions can be discovered without any deterioration in terms of training time or test accuracy (Frankle & Carbin, 2019). However, for more realistic architectures such as *ResNets*, the picture changes and subnetworks can only be identified if the employed learning rate is small enough. As a remedy, Frankle et al. (2020a) add the following modification to the above strategy: Instead of rewinding back to the initialization $\theta^{(0)}$ and applying the pruning there, another checkpoint $\theta^{(l)}$ early in training is used and $m \odot \theta^{(l)}$ is re-trained instead of $m \odot \theta^{(0)}$. Frankle et al. (2020a) show that checkpoints as early as 1 epoch can suffice to identify lottery tickets, even at standard learning rates. Interestingly, Frankle et al. (2020a) further show that the point in time l where lottery tickets can be found, coincides with the time where SGD becomes stable to different batch orderings π , i.e. different runs of SGD with distinct batch orderings but the same initialization $\theta^{(l)}$ end up in the same linear basin. This property is also called linear mode connectivity; we provide an illustration in Fig. 8. Notice that in general, linear mode-connectivity does not hold, i.e. two SGD runs from the same initialization end up in two disconnected basins (Frankle et al., 2020a; Garipov et al., 2018).

IMP from student. A natural question that emerges now is whether a student checkpoint θ_S^* obtained through random teacher distillation already developed sparse structures in the form of lottery tickets. Closely following the setup in Frankle et al. (2020a), we compare the robustness of rewinding points $\theta^{(l)}$ with our student checkpoints θ_S^* (we focus on $\alpha = 0$ in this section). We display the results

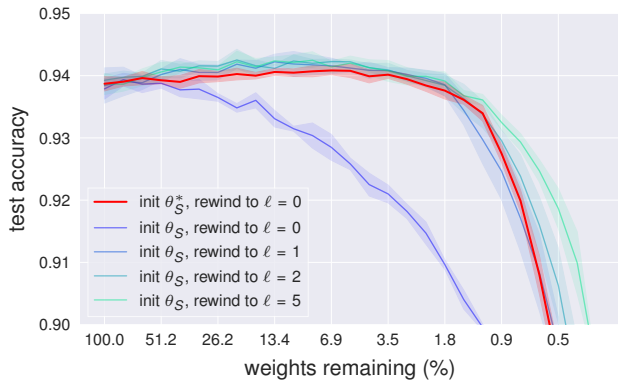


Figure 9. Test accuracy as a function of sparsity for different initialization and rewinding strategies. Fresh initializations θ_S are not robust to IMP with rewinding to initialization ($l = 0$), this only emerges with rewinding to $l \geq 1$. Student checkpoints θ_S^* are always robust to IMP even with rewinding to $l = 0$. One epoch corresponds to 196 steps. Aggregation is done over 5 checkpoints.

in Fig. 9, where we plot test performance on *CIFAR10* as a function of the sparsity level. We use a *ResNet18* and iterative magnitude pruning, reducing the network by a fraction of 0.2 every round. We compare against rewinding to supervised checkpoints $\theta^{(l)}$ for $l \in \{0, 1, 2, 5\}$ where l is measured in number of epochs. We observe that rewinding to $l = 0$, as shown in Frankle & Carbin (2019); Frankle et al. (2020a), incurs strong losses in terms of test accuracy at all pruning levels and thus does not constitute a lottery ticket. The distilled student θ_S^* on the other hand remains very robust to strong degrees of pruning and shows a similar behaviour to the networks rewound to later checkpoints, thus constituting a valid ticket. We re-iterate here that the student has not seen any target information but is simply distilled from a random teacher without any structure. Similarly to previous experiments, the simple implicit regularization present in the learning dynamics of SGD suffices to find meaningful, data-dependent representations. This is in line with results in Frankle et al. (2020b) that show that auxiliary tasks such as rotation prediction can lead to lottery tickets. We emphasize however that our setup completely lacks any data-informed bias such as rotations.

Linear mode connectivity. In light of the observation regarding the stability of SGD in Frankle et al. (2020a), it is natural to verify whether a similar stability property holds for the student checkpoint θ_S^* . To that end, we train several runs of SGD in a supervised fashion with initialization θ_S^* and different batch orderings π_1, \dots, π_b and study the test accuracies occurred along linear paths between different solutions $\theta_{\pi_i}^*$ for $i = 1, \dots, b$, i.e.

$$\theta_{\pi_i \rightarrow \pi_j}(\gamma) := \gamma \theta_{\pi_i}^* + (1 - \gamma) \theta_{\pi_j}^*.$$

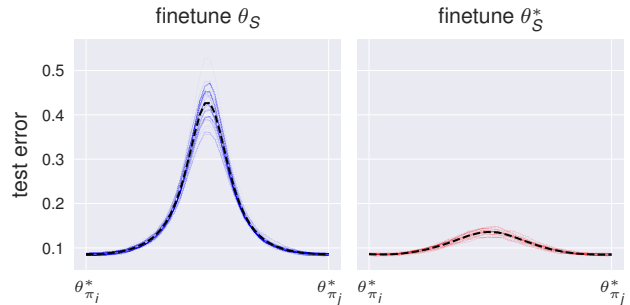


Figure 10. Test error when interpolating between networks that were finetuned from the same checkpoint. **Left:** Networks initialized at random, i.e. the untrained student θ_S . **Right:** Networks initialized with the converged student checkpoint θ_S^* . Aggregation is done over 3 checkpoints and 5 different data orderings π_i .

If the test accuracy along the path does not significantly worsen, we call $\theta_{\pi_i}^*$ and $\theta_{\pi_j}^*$ linearly mode-connected. We contrast the results with the interpolation curves for SGD runs started from the same, *random* initialization. We display the interpolation curves in Fig. 10. We used a *ResNet18* student, distilled on *CIFAR10* from a random teacher and finetuned three networks subsequently with SGD. We see that indeed, the resulting parameters $\theta_{\pi_i}^*$ all lie in approximately the same linear basin. The networks trained from the random initialization however face a significantly larger barrier.

7. Discussion and Conclusion

In this work we examined the teacher-student setting more closely, with the aim of disentangling its implicit regularization from other very common components such as dark knowledge in trained teachers and the implicit bias in learning invariances with respect to data augmentations. We showed that surprisingly, students manage to learn strong structures even from random teachers in the absence of data augmentation. We studied the quality of the resulting student representations and observed that (1) probing accuracies significantly improve over the teacher, (2) features are transferable across tasks and (3) lottery tickets can be identified based on the student checkpoints without training on the supervised task. The successes of teacher-student-based pipelines such as knowledge distillation and non-contrastive learning can thus at least partially be attributed to the regularizing nature of the learning dynamics.

In summary, we find that even if the teacher is completely data-agnostic, training dynamics exhibit a remarkable regularizing effect, mimicking the very early phase of supervised training to a surprising degree. The simple and minimal nature of our setting makes it an ideal test bed for better understanding this early phase of learning. We hope that future theoretical work can build upon our simplified framework.

References

- Allen-Zhu, Z. and Li, Y. Towards understanding ensemble, knowledge distillation and self-distillation in deep learning. *ArXiv*, abs/2012.09816, 2020.
- Anagnostidis, S., Bachmann, G., Noci, L., and Hofmann, T. The curious case of benign memorization. 2022. doi: 10.48550/ARXIV.2210.14019. URL <https://arxiv.org/abs/2210.14019>.
- Assran, M., Caron, M., Misra, I., Bojanowski, P., Bordes, F., Vincent, P., Joulin, A., Rabbat, M., and Ballas, N. Masked Siamese Networks for Label-Efficient Learning. 4 2022. doi: 10.48550/arxiv.2204.07141. URL <https://arxiv.org/abs/2204.07141v1>.
- Ba, J. and Caruana, R. Do deep nets really need to be deep? In *NIPS*, 2013.
- Bardes, A., Ponce, J., and LeCun, Y. VICReg: Variance-invariance-covariance regularization for self-supervised learning. In *International Conference on Learning Representations (ICLR)*, 2022.
- Bucila, C., Caruana, R., and Niculescu-Mizil, A. Model compression. In *Knowledge Discovery and Data Mining*, 2006.
- Caron, M., Touvron, H., Misra, I., Jégou, H., Mairal, J., Bojanowski, P., and Joulin, A. Emerging properties in self-supervised vision transformers. *2021 IEEE/CVF International Conference on Computer Vision (ICCV)*, pp. 9630–9640, 2021a.
- Caron, M., Touvron, H., Misra, I., Jégou, H., Mairal, J., Bojanowski, P., and Joulin, A. Emerging properties in self-supervised vision transformers. In *Proceedings of the IEEE/CVF International Conference on Computer Vision*, pp. 9650–9660, 2021b.
- Chen, G., Choi, W., Yu, X., Han, T., and Chandraker, M. Learning efficient object detection models with knowledge distillation. In Guyon, I., Luxburg, U. V., Bengio, S., Wallach, H., Fergus, R., Vishwanathan, S., and Garnett, R. (eds.), *Advances in Neural Information Processing Systems*, volume 30. Curran Associates, Inc., 2017. URL <https://proceedings.neurips.cc/paper/2017/file/e1e32e235eeelf970470a3a6658dfdd5-Paper.pdf>.
- Chen, T., Kornblith, S., Norouzi, M., and Hinton, G. A simple framework for contrastive learning of visual representations. In III, H. D. and Singh, A. (eds.), *Proceedings of the 37th International Conference on Machine Learning*, volume 119 of *Proceedings of Machine Learning Research*, pp. 1597–1607. PMLR, 13–18 Jul 2020.
- Chen, X. and He, K. Exploring Simple Siamese Representation Learning. *Proceedings of the IEEE Computer Society Conference on Computer Vision and Pattern Recognition*, pp. 15745–15753, 11 2020. ISSN 10636919. doi: 10.48550/arxiv.2011.10566. URL <https://arxiv.org/abs/2011.10566v1>.
- Chen, X. and He, K. Exploring simple siamese representation learning. In *Proceedings of the IEEE/CVF Conference on Computer Vision and Pattern Recognition*, pp. 15750–15758, 2021.
- Coates, A., Ng, A., and Lee, H. An analysis of single-layer networks in unsupervised feature learning. In Gordon, G., Dunson, D., and Dudík, M. (eds.), *Proceedings of the Fourteenth International Conference on Artificial Intelligence and Statistics (AISTATS)*, volume 15 of *Proceedings of Machine Learning Research*, pp. 215–223, Fort Lauderdale, FL, USA, 11–13 Apr 2011. PMLR.
- Devlin, J., Chang, M.-W., Lee, K., and Toutanova, K. BERT: Pre-training of deep bidirectional transformers for language understanding. In *Proceedings of the 2019 Conference of the North American Chapter of the Association for Computational Linguistics: Human Language Technologies, Volume 1 (Long and Short Papers)*, pp. 4171–4186, Minneapolis, Minnesota, June 2019. Association for Computational Linguistics. doi: 10.18653/v1/N19-1423. URL <https://aclanthology.org/N19-1423>.
- Draxler, F., Veschgini, K., Salmhofer, M., and Hamprecht, F. Essentially no barriers in neural network energy landscape. In *International conference on machine learning*, pp. 1309–1318. PMLR, 2018.
- Frankle, J. and Carbin, M. The lottery ticket hypothesis: Finding sparse, trainable neural networks. In *International Conference on Learning Representations*, 2019. URL <https://openreview.net/forum?id=rJl-b3RcF7>.
- Frankle, J., Dziugaite, G. K., Roy, D., and Carbin, M. Linear mode connectivity and the lottery ticket hypothesis. In III, H. D. and Singh, A. (eds.), *Proceedings of the 37th International Conference on Machine Learning*, volume 119 of *Proceedings of Machine Learning Research*, pp. 3259–3269. PMLR, 13–18 Jul 2020a. URL <https://proceedings.mlr.press/v119/frankle20a.html>.
- Frankle, J., Schwab, D. J., and Morcos, A. S. The early phase of neural network training. In *International Conference on Learning Representations*, 2020b. URL <https://openreview.net/forum?id=Hk1liRNFwS>.
- Furlanello, T., Lipton, Z. C., Tschannen, M., Itti, L., and Anandkumar, A. Born again neural networks. In *International Conference on Machine Learning*, 2018.

- Garipov, T., Izmailov, P., Podoprikin, D., Vetrov, D., and Wilson, A. G. Loss surfaces, mode connectivity, and fast ensembling of dnns. In *Proceedings of the 32nd International Conference on Neural Information Processing Systems*, NIPS'18, pp. 8803–8812, Red Hook, NY, USA, 2018. Curran Associates Inc.
- Grill, J.-B., Strub, F., Alché, F., Tallec, C., Richemond, P., Buchatskaya, E., Doersch, C., Avila Pires, B., Guo, Z., Gheshlaghi Azar, M., et al. Bootstrap your own latent—a new approach to self-supervised learning. *Advances in neural information processing systems*, 33:21271–21284, 2020.
- He, H., Huang, G., and Yuan, Y. Asymmetric valleys: Beyond sharp and flat local minima. In Wallach, H., Larochelle, H., Beygelzimer, A., d'Alché-Buc, F., Fox, E., and Garnett, R. (eds.), *Advances in Neural Information Processing Systems*, volume 32. Curran Associates, Inc., 2019a. URL <https://proceedings.neurips.cc/paper/2019/file/01d8bae291b1e4724443375634ccfa0e-Paper.pdf>.
- He, H., Huang, G., and Yuan, Y. Asymmetric valleys: Beyond sharp and flat local minima. *33rd Conference on Neural Information Processing Systems (NeurIPS)*, 2019b.
- He, K., Zhang, X., Ren, S., and Sun, J. Delving deep into rectifiers: Surpassing human-level performance on imagenet classification. In *2015 IEEE International Conference on Computer Vision (ICCV)*, pp. 1026–1034, Los Alamitos, CA, USA, dec 2015. IEEE Computer Society. doi: 10.1109/ICCV.2015.123. URL <https://doi.ieeecomputersociety.org/10.1109/ICCV.2015.123>.
- He, K., Zhang, X., Ren, S., and Sun, J. Deep residual learning for image recognition. *IEEE Conference on Computer Vision and Pattern Recognition (CVPR)*, 2016.
- Hinton, G. E., Vinyals, O., and Dean, J. Distilling the knowledge in a neural network. *ArXiv*, abs/1503.02531, 2015.
- Ioffe, S. and Szegedy, C. Batch normalization: Accelerating deep network training by reducing internal covariate shift. In Bach, F. and Blei, D. (eds.), *Proceedings of the 32nd International Conference on Machine Learning*, volume 37 of *Proceedings of Machine Learning Research*, pp. 448–456, Lille, France, 07–09 Jul 2015. PMLR. URL <https://proceedings.mlr.press/v37/ioffe15.html>.
- Izmailov, P., Vikram, S., Hoffman, M. D., and Wilson, A. G. G. What are bayesian neural network posteriors really like? In Meila, M. and Zhang, T. (eds.), *Proceedings of the 38th International Conference on Machine Learning*, volume 139 of *Proceedings of Machine Learning Research*, pp. 4629–4640. PMLR, 18–24 Jul 2021. URL <https://proceedings.mlr.press/v139/izmailov21a.html>.
- Jacot, A., Gabriel, F., and Hongler, C. Neural tangent kernel: Convergence and generalization in neural networks. *Advances in neural information processing systems*, 31, 2018.
- Ji, G. and Zhu, Z. Knowledge distillation in wide neural networks: Risk bound, data efficiency and imperfect teacher. *Advances in Neural Information Processing Systems*, 33: 20823–20833, 2020.
- Kingma, D. P. and Ba, J. Adam: A method for stochastic optimization. *International Conference on Learning Representations (ICLR)*, 2017.
- Krizhevsky, A. and Hinton, G. Learning multiple layers of features from tiny images. Technical Report 0, University of Toronto, Toronto, Ontario, 2009.
- Le, Y. and Yang, X. Tiny imagenet visual recognition challenge. *CS 231N*, 7(7):3, 2015.
- Li, H., Xu, Z., Taylor, G., Studer, C., and Goldstein, T. Visualizing the loss landscape of neural nets. In *Proceedings of the 32nd International Conference on Neural Information Processing Systems*, NIPS'18, pp. 6391–6401, Red Hook, NY, USA, 2018. Curran Associates Inc.
- Mobahi, H., Farajtabar, M., and Bartlett, P. L. Self-distillation amplifies regularization in hilbert space. In *Proceedings of the 34th International Conference on Neural Information Processing Systems*, NIPS'20, Red Hook, NY, USA, 2020. Curran Associates Inc. ISBN 9781713829546.
- Nagarajan, V. and Kolter, J. Z. Uniform convergence may be unable to explain generalization in deep learning. *33rd Conference on Neural Information Processing Systems (NeurIPS)*, 2019.
- Nakkiran, P., Neyshabur, B., and Sedghi, H. The deep bootstrap framework: Good online learners are good offline generalizers. In *International Conference on Learning Representations*, 2021. URL <https://openreview.net/forum?id=guetrIHLFGI>.
- Phuong, M. and Lampert, C. Towards understanding knowledge distillation. In *International Conference on Machine Learning*, pp. 5142–5151. PMLR, 2019.

- Polino, A., Pascanu, R., and Alistarh, D. Model compression via distillation and quantization. In *International Conference on Learning Representations*, 2018. URL <https://openreview.net/forum?id=S1XolQbRW>.
- Schroff, F., Kalenichenko, D., and Philbin, J. Facenet: A unified embedding for face recognition and clustering. In *2015 IEEE Conference on Computer Vision and Pattern Recognition (CVPR)*, pp. 815–823, 2015. doi: 10.1109/CVPR.2015.7298682.
- Simonyan, K. and Zisserman, A. Very deep convolutional networks for large-scale image recognition. *International Conference on Learning Representations (ICLR)*, 2014.
- Tarvainen, A. and Valpola, H. Mean teachers are better role models: Weight-averaged consistency targets improve semi-supervised deep learning results. *31st Conference on Neural Information Processing Systems (NeurIPS)*, 30, 2017.
- Tian, Y., Chen, X., and Ganguli, S. Understanding self-supervised learning dynamics without contrastive pairs. In *International Conference on Machine Learning*, pp. 10268–10278. PMLR, 2021.
- van den Oord, A., Li, Y., and Vinyals, O. Representation learning with contrastive predictive coding. *ArXiv*, abs/1807.03748, 2018.
- Wang, X., Chen, X., Du, S. S., and Tian, Y. Towards demystifying representation learning with non-contrastive self-supervision, 2022. URL https://openreview.net/forum?id=yCS5dckx_vj.
- Wang, Y., Li, H., Chau, L.-p., and Kot, A. C. Embracing the dark knowledge: Domain generalization using regularized knowledge distillation. In *Proceedings of the 29th ACM International Conference on Multimedia*, MM ’21, pp. 2595–2604, New York, NY, USA, 2021. Association for Computing Machinery. ISBN 9781450386517. doi: 10.1145/3474085.3475434. URL <https://doi.org/10.1145/3474085.3475434>.
- Xu, K., Park, D. H., Yi, C., and Sutton, C. Interpreting deep classifier by visual distillation of dark knowledge. 03 2018.
- Yang, C., Xie, L., Su, C., and Yuille, A. L. Snapshot distillation: Teacher-student optimization in one generation. *2019 IEEE/CVF Conference on Computer Vision and Pattern Recognition (CVPR)*, pp. 2854–2863, 2018.
- Yim, J., Joo, D., Bae, J., and Kim, J. A gift from knowledge distillation: Fast optimization, network minimization and transfer learning. In *Proceedings of the IEEE Conference on Computer Vision and Pattern Recognition (CVPR)*, July 2017.
- Yuan, L., Tay, F. E., Li, G., Wang, T., and Feng, J. Revisiting knowledge distillation via label smoothing regularization. In *Proceedings of the IEEE/CVF Conference on Computer Vision and Pattern Recognition*, pp. 3903–3911, 2020.
- Zbontar, J., Jing, L., Misra, I., LeCun, Y., and Deny, S. Barlow twins: Self-supervised learning via redundancy reduction. In *International Conference on Machine Learning*, pp. 12310–12320. PMLR, 2021.
- Zhang, C., Zhang, K., Zhang, C., Pham, T. X., Yoo, C. D., and Kweon, I. S. How does simsiam avoid collapse without negative samples? a unified understanding with self-supervised contrastive learning. In *International Conference on Learning Representations*, 2022. URL <https://openreview.net/forum?id=bwq604Cwdl>.
- Zhang, L., Song, J., Gao, A., Chen, J., Bao, C., and Ma, K. Be your own teacher: Improve the performance of convolutional neural networks via self distillation. *2019 IEEE/CVF International Conference on Computer Vision (ICCV)*, pp. 3712–3721, 2019.

A. The Algorithm

Distillation from a random teacher has two important details. The outputs are very high-dimensional, 2^{16} -d. And a special component, the *l2-bottleneck*, is hidden in the architecture of the projection head just before the softmax. It linearly maps a feature vector to a low-dimensional space, normalizes it and computes the dot product with a normalized weight matrix, i.e.

$$x \rightarrow \tilde{V}^T \frac{W^T x + b}{\|W^T x + b\|_2} \text{ with } \|\tilde{V}_{:,i}\|_2 = 1$$

for $x \in \mathbb{R}^n$, $W \in \mathbb{R}^{n \times k}$, $b \in \mathbb{R}^k$, $\tilde{V} \in \mathbb{R}^{k \times m}$. This architecture is heavily inspired by DINO (Caron et al., 2021b). Let us summarize the method in pseudo-code:

```

encoder, head, wn_layer = ResNet(512), MLP(2048,2048,256), Linear(216)

student = initialize(encoder, head, wn_layer)
teacher = copy(student) # initialize with same parameters
for x, y in repeat(data, n_epochs):
    # apply weight-normalization
    normalized_weight_t = normalize(teacher.wn_layer.weight)
    normalized_weight_s = normalize(student.wn_layer.weight)

    # prepare target
    x_t = teacher.head(teacher.encoder(x))
    x_t = normalize(x_t)
    x_t = dot(normalized_weight_t, x_t)
    target = softmax(x_t)

    # prepare prediction
    x_s = student.head(student.encoder(x))
    x_s = normalize(x_s)
    x_s = dot(normalized_weight_s, x_s)
    prediction = softmax(x_s)

    # compute loss, backpropagate and update
    loss = sum(target * -log(prediction)) # cross-entropy
    loss.backward()
    optimizer.step(student) # update only student

```

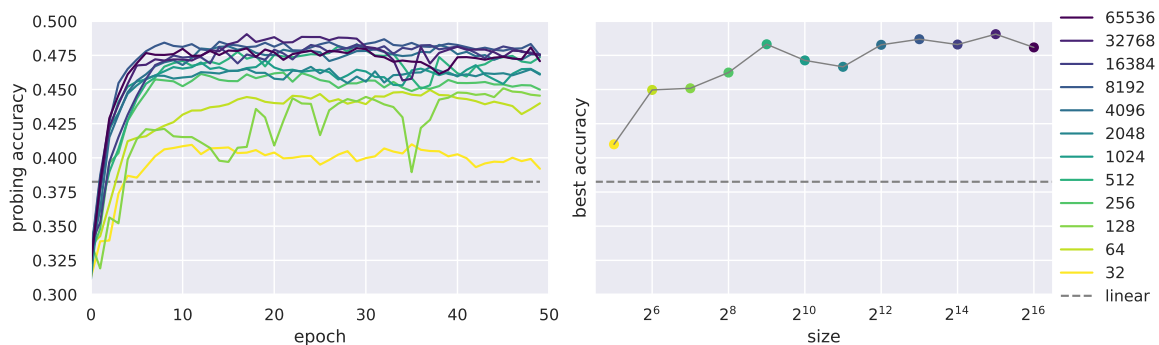


Figure 11. Random teacher distillation for increasing output dimension (*ResNet18* on *CIFAR10*). **Left:** Probing accuracy during training. **Right:** Best probe vs output dimension.

B. Ablating the Architecture

B.1. Ablating Encoder Normalization Layers

If the teacher is used in evaluation mode, then one possible source of asymmetry is introduced by batch normalization layers. But is the effect caused by this batch-dependent signal? Or does the batch dependency amplify the mechanism? In Fig. 12 we compare different types of normalization layers and no normalization (Identity). We observe that although BN stabilizes training, the effect occurs also with batch-independent normalization. Further, networks without normalization reach similar performance but take longer to converge.

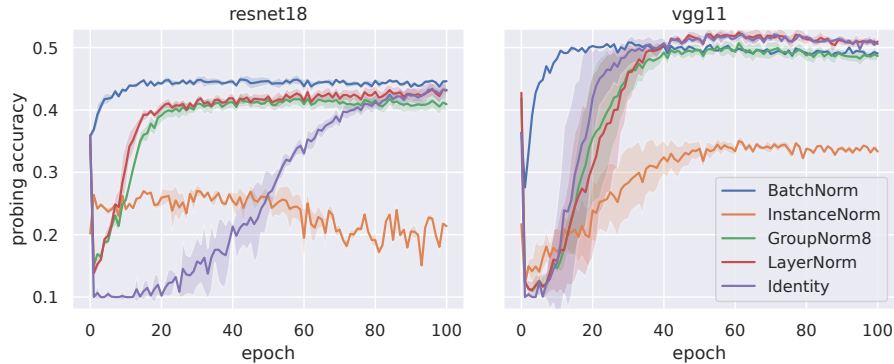


Figure 12. Comparing different types of normalization layers (*ResNet18*, *VGG11* on *CIFAR10*)

B.2. Ablating the Projector L2-Bottleneck

The *l2-Bottleneck* is a complex layer with many unexplained design choices. We compare different combinations of weight-normalization (wn), linear layer (lin), and feature normalization (fn) for the first and second part of the bottleneck in Figures 13 and 14 for a *ResNet18* and a *VGG11* respectively. While the default setup is clearly the most performant, removing feature normalization is more destructive than removing weight normalization. In particular, only one linear layer followed by a feature normalization still exhibits a similar trend and does not break down.

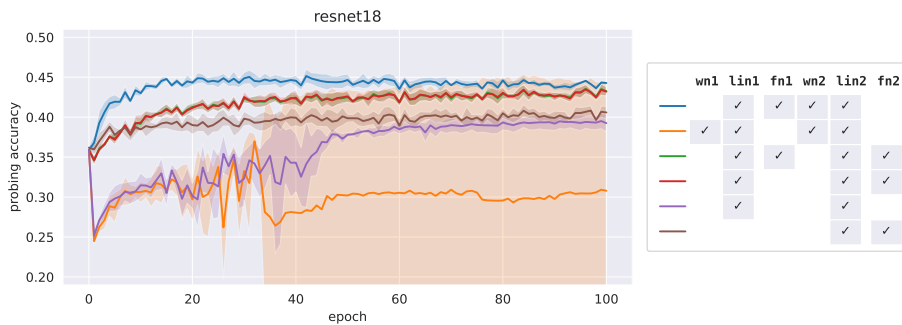


Figure 13. Ablating components of the *l2-bottleneck* (*ResNet18* on *CIFAR10*).

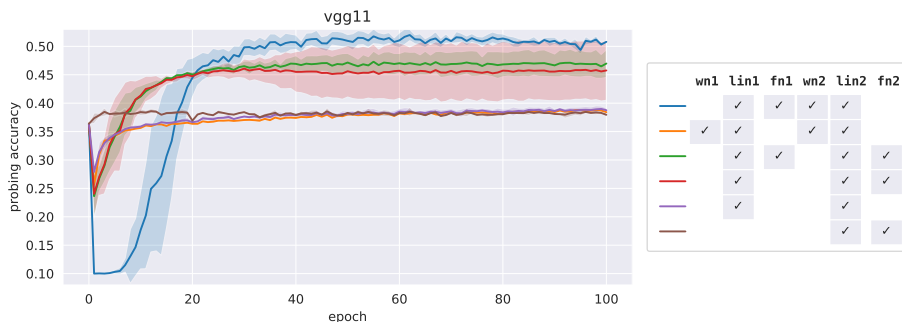


Figure 14. Ablating components of the *l2-bottleneck* (*VGG11* on *CIFAR10*).

C. Experimental Details

Our main goal is to demystify the properties of distillation in a simplistic setting, removing a series of ‘tricks’ used in practice. For clarity reasons, we here present a comprehensive comparison with the popular framework of DINO (Caron et al., 2021b).

C.1. Architecture

Configuration	
Encoder	ResNet18&VGG1 from torchvision, without fc or classification layers (embedding $\in \mathbb{R}^{512}$) (ResNet18 adjusted stem for CIFAR: conv from 7x7 to 3x3, remove maxpool)
Projection Head	3-Layer MLP: $512 \rightarrow 2048 \rightarrow 2048 \rightarrow \text{l2-bottleneck}(256) \rightarrow 2^{16}$ (GELU activation, no batchnorms, init: trunc_normal with $\sigma = 0.02$, biases=0)
L2-Bottleneck(in, mid, out)	for $x \in \mathbb{R}^{in}$, $W \in \mathbb{R}^{in \times mid}$, $b \in \mathbb{R}^{mid}$, $\tilde{V} \in \mathbb{R}^{mid \times out}$ 1. linear to bottleneck: $z = W^T x + b \in \mathbb{R}^{mid}$ 2. feature normalization: $\tilde{z} = z / \ z\ _2$ 3. weightnormalized linear: $y = \tilde{V}^T \tilde{z} \in \mathbb{R}^{out}$, with $\ \tilde{V}_{:,i}\ _2 = 1$ $\Rightarrow f_{\tilde{V},W}(x) = \tilde{V}^T \frac{W^T x + b}{\ W^T x + b\ _2}$ with $\ \tilde{V}_{:,i}\ _2 = 1$

C.2. Data

Configuration	DINO default	Random Teacher
Augmentations	Multicrop ($2 \times 224^2 + 10 \times 96^2$) + SimCLR-like	None (1×32^2)
Training batchsize	64 per GPU	256
Evaluation batchsize	128 per GPU	256

C.3. DINO Hyperparameters

Configuration	DINO default	Random Teacher Distillation
Teacher update	ema with momentum $0.996 \xrightarrow{cos} 1$	no updates
Teacher BN update	BN in train mode	BN in eval mode
Teacher centering	track statistics with momentum 0.9	not applied
Teacher sharpening	temperature 0.04 (paper: $0.04 \xrightarrow{lin} 0.07$)	temperature 1
Student sharpening	temperature 0.1	temperature 1
Loss function	opposite-crop cross-entropy	single-crop cross-entropy

C.4. Random Teacher Distillation

Configuration	DINO default	Random Teacher Distillation
Optimizer	AdamW	AdamW
Learning rate	$0 \xrightarrow{lin} 0.0005 \xrightarrow{cos} 1e-6$ schedule	0.001 (torch default)
Weight decay	$0.04 \xrightarrow{lin} 0.4$ schedule	not applied
Gradient Clipping	to norm 3	not applied
Freezing of last layer	during first epoch	not applied

C.5. IMP Supervised Training

Configuration	Lottery Ticket Hypothesis (Frankle et al., 2020b)	IMP on student checkpoints
Training Epochs	160	160
Optimizer	SGD (momentum 0.9)	SGD (momentum 0.9)
Learning rate	MultiStep: $0.1 \xrightarrow{80 \text{ epochs}} 0.01 \xrightarrow{40 \text{ epochs}} 0.001$	MultiStep: $0.1 \xrightarrow{80 \text{ epochs}} 0.01 \xrightarrow{40 \text{ epochs}} 0.001$
Weight decay	0.0001	0.0001
Augmentations	Random horizontal flip & padded crop (4px)	Random horizontal flip & padded crop (4px)

D. Additional Results

We present additional experimental results that serve to better understand the regularization properties of self-distillation with random teachers.

D.1. K -NN probing

A different probing choice instead of learning a linear layer on top of the extracted embeddings is to perform K -NN classification on the features. We apply K -nearest-neighbour classification with the number of neighbours set to $K = 20$, as commonly done in practice. As in Table 1 in the main text, we present results under K -NN evaluation in Table 3. Also, as in Table 2, we evaluate using K -NN probing the transferability of the learnt embeddings from *TinyImageNet* in Table 4.

DATASET	MODEL	TEACHER	STUDENT	INPUT
<i>CIFAR10</i>	<i>ResNet18</i>	37.65	44.67	
	<i>VGG11</i>	44.92	51.32	33.61
<i>CIFAR100</i>	<i>ResNet18</i>	13.77	20.22	
	<i>VGG11</i>	18.10	23.53	14.87
<i>STL10</i>	<i>ResNet18</i>	31.71	37.41	
	<i>VGG11</i>	36.92	43.58	28.94
<i>TinyImageNet</i>	<i>ResNet18</i>	4.59	7.11	
	<i>VGG11</i>	5.98	9.23	3.44

Table 3. K -NN probing accuracies (in percentage) of the representations for various datasets for teacher, student and raw pixel inputs.

DATASET	MODEL	TEACHER	STUDENT
<i>CIFAR10</i>	<i>ResNet18</i>	37.65	44.45
	<i>VGG11</i>	44.92	51.48
<i>CIFAR100</i>	<i>ResNet18</i>	13.77	19.48
	<i>VGG11</i>	18.10	23.95
<i>STL10</i>	<i>ResNet18</i>	31.71	38.86
	<i>VGG11</i>	36.92	42.26

Table 4. K -NN probing accuracies (in percentage) of the representations for various datasets for teacher, student when transferred from *TinyImageNet*

D.2. Loss landscapes

The parameter plane visualized in Fig. 6 is defined by interpolation between three parameterizations, thus distances and angles are not preserved. In the following Fig. 15, we orthogonalize the basis of the parameter plane to achieve a distance and angle-preserving visualization. We note that both converged solutions of the students $\Theta_{S_0^*}$ and $\Theta_{S_1^*}$ stay comparably close to their initializations. Further, we provide a zoomed crops the asymmetric valley around the teacher Θ_{S_T} in Fig. 16.

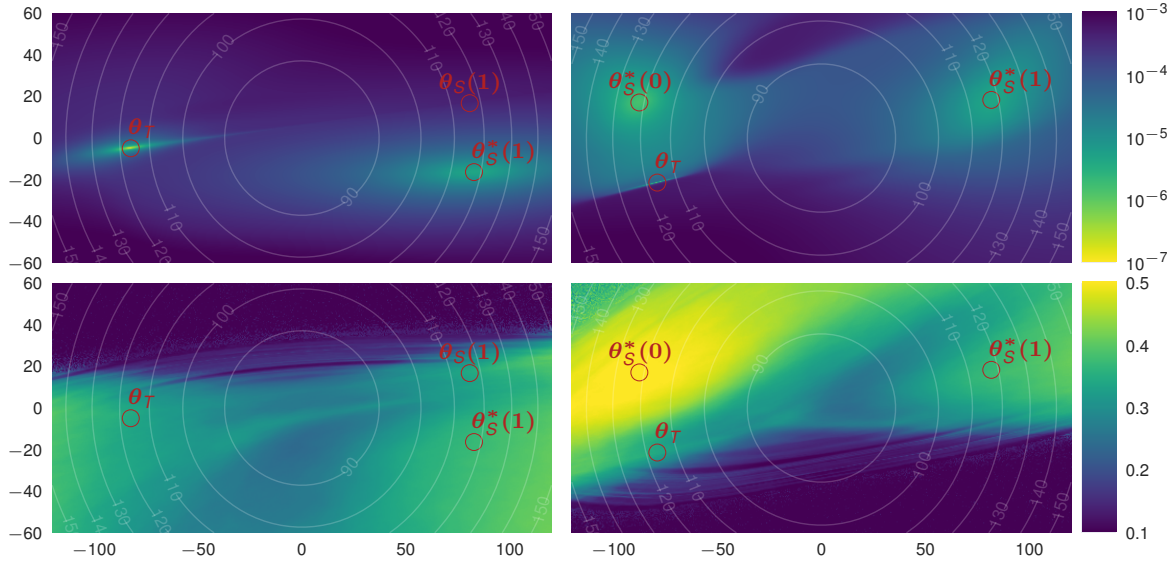


Figure 15. Orthogonal projection of the loss landscape in the parameter plane.

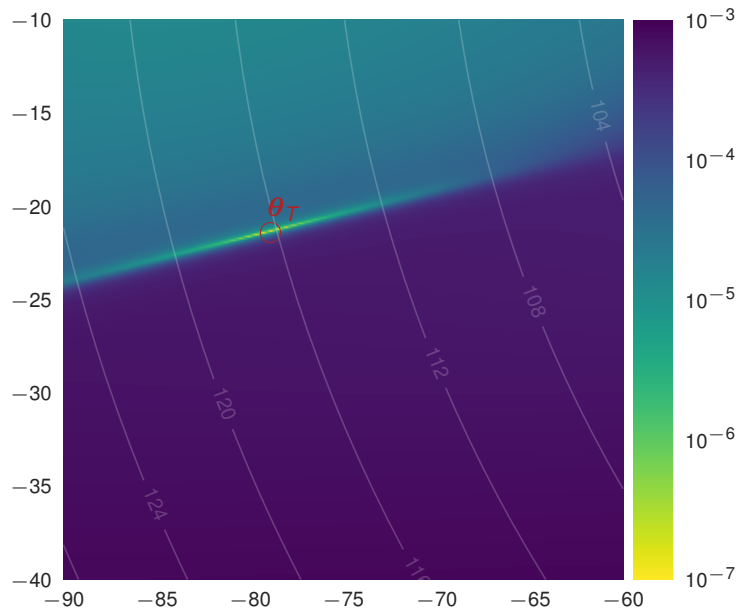


Figure 16. Higher resolution crop of the global optimum around the teacher.

The same visualization technique allows plotting the KL divergence between embeddings produced by the teacher and other parametrization in the plane. While in Fig.15, the basin of the local solution matches with the area of increased probing accuracy, such a correlation is not visible if one only considers the encoder.

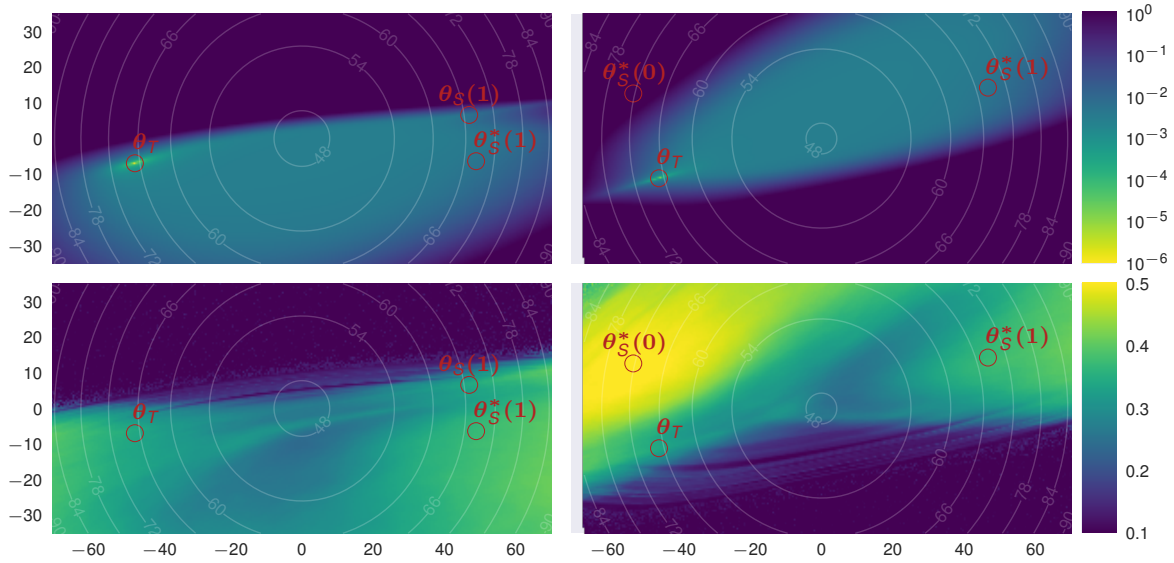


Figure 17. Orthogonal projection of the embedding KL divergence landscape in the parameter plane.

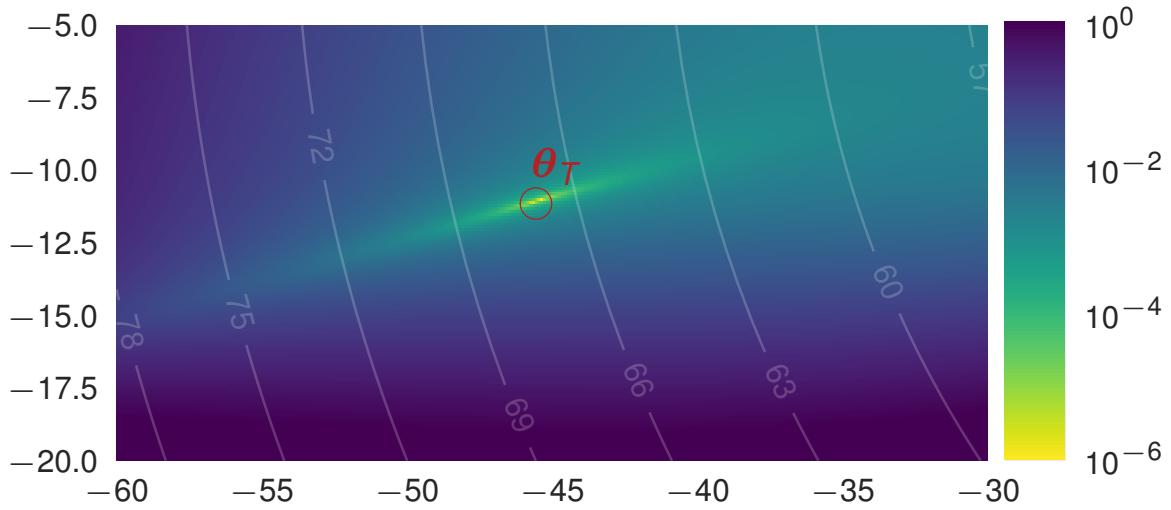


Figure 18. Higher resolution crop of the global optimum around the teacher.